2022 IEEE International Conference on Robotics and Automation (ICRA)
May 23-27, 2022. Philadelphia, PA, USA

Toward Physical Human-Robot Interaction Control with Aerial Manipulators: Compliance, Redundancy Resolution, and Input Limits

Amr Afifi[1], Mark van Holland[1], Antonio Franchi[1,2]

***Abstract*— In this paper we introduce a comprehensive framework to control an aerial manipulator, i.e., an aerial vehicle with a robotic arm, in physical interaction with a human operator or co-worker. The framework uses an admittance control paradigm in order to attain human ergonomy and safety; an interaction supervisor to automatically shape the compliance based on the interaction regions defined around the human co-worker; a projected gradient redundancy resolution scheme to exploit the multiple degrees of freedom of the aerial robot to accommodate for possible additional secondary tasks; and a quadratic programming optimization-based inner loop to cope with real world input saturation and increase the safety level of the human co-worker. The control framework is demonstrated and validated through numerical simulations with a human-in-the loop.**

I. Introduction

Advances in Aerial Robotics research in recent years have shown both the viability and effectiveness of using aerial robots with various designs, including, e.g., aerial manipulators, in tasks that require physical interaction with the environment [1], [2]. In particular, aerial manipulators, with both fully actuated and under-actuated configurations are showing great promise in very complex physical [3], [4] and motion tasks [5]. In parallel, the domain of safe *physical Human Robot Interaction* (pHRI), specifically in the realm of fixed base manipulators, has been studied extensively over the last two decades [6]–[8], and it is steadily becoming a reality with numerous examples outside lab environments in addition to evolving ISO standards and specifications that allow for more interaction between human operators and robotic co-workers.

The advances done in aerial robotics with regards to physical interaction with the environment has also sparked the idea of aerial robots interacting with humans at elevated places. One can envision aerial robots of the future performing tool deliveries or some cooperative tasks with a human operator which are working at height. Up till now, the idea has been investigated only briefly in aerial robotics literature with just a handful of results. In [9] the suitability of an admittance control scheme to physical human-quadrotor interaction is shown, where a human guides a quadrotor carrying a foam brick. In [10], collision detection and reaction techniques, presented in [6] for fixed base manipulators, are extended to aerial robots to increase safety. Additionally, a comparison between impedance and admittance control is performed for a quadrotor. In [11], a human interacts with an aerial vehicle via a cable in which again an admittance control scheme is used for safe pHRI. In [12] the long reach configuration – consisting of a dual arm aerial manipulator suspended with a passive bar – is used to perform a tool delivery. One can see that in [9], [10] and [11] the human interacts with the aerial vehicle through the air frame or a cable, which limits the applications of the interaction to physically guiding the aerial vehicle in the air. Some works in aerial robotics have also investigated the problem of cognitive interaction between an aerial robot and a human operator, for example in [13] sensory devices such as eye tracking glasses and an inertial measurement unit are used for a human to give spatial tasks to an aerial robot.

Safety is of paramount importance during pHRI. A human interacting with the robot should feel safe with respect to the robot mechanical design (e.g., moving parts like propellers) and the robot motion (e.g., proximity to the human). Additionally, the robot should not, under any circumstance, cause injury to the interacting human. As mentioned earlier, literature on safe pHRI, tackles these different aspects of safety, but with a clear focus toward manipulators on a fixed base. A fundamental difference between fixed base manipulators and their aerial counterparts are the actuation capabilities, which has implications on safety in pHRI. Firstly, aerial manipulators that can be used in the proximity of a human operator are extremely constrained in the available energy ad power. Most of their actuation strength is used for gravity compensation. The remaining part of the actuation that can be used for physical interaction is in general much lower than the one a human collaborator can exert on the system. As a consequence it is much harder for an aerial manipulator controller to implement a correct and safe interaction behavior because the actuation subsystem is continuously prone to be pushed to its limits. Therefore, we believe that designing a controller that can minimize the divergence from the predefined safe interaction behavior, in the case of control input saturation, is an important step toward safe aerial pHRI. Secondly, in dangerous situations a fixed base manipulator can be stopped by applying brakes or high gain feedback, on the other hand, an aerial manipulator obviously can not be turned off in midair. These two important aspects led us to conclude that for obtaining a safe and ergonomic *human-aerial robot interaction*, an interaction control control scheme must take into account actuation limits explicitly. This is in line with a recent trend – in aerial robotics – that promotes the use of optimization-based control to pursue

[1]Robotics and Mechatronics lab, Faculty of Electrical Engineering, Mathematics & Computer Science, University of Twente, Enschede, The Netherlands, a.n.m.g.afifi@utwente.nl, m.vanholland@student.utwente.nl, a.franchi@utwente.nl
[2]LAAS-CNRS, Université de Toulouse, CNRS, Toulouse, France,
This work was partially funded by European Commission project H2020 AERIAL-CORE (EC 871479).

2022 IEEE International Conference on Robotics and Automation (ICRA) | 978-1-7281-9681-7/22/$31.00 ©2022 IEEE | DOI: 10.1109/ICRA46639.2022.9812451

Fig. 1: Example of AM: the *aerial manipulator* at RAM-UT, with a fully actuated hexarotor aerial vehicle and a 3-DoF arm, thus 9-DoFs in total.

various objectives while including explicitly the actuation limits [14], [15].

In this work, we propose what we believe is at date the most complete physical interaction control scheme for aerial manipulators that is suitable for safe and ergonomic human-aerial-robot physical interaction tasks. The method has the following features. First of all, in light of the previous considerations, it embraces explicitly the input bounds in its formulation. Second of all it exploits the redundancy of the aerial manipulator in order to attain possible secondary tasks. Finally, it allows a compliant and safe physical interaction with a human operator. The last two features represent a substantial improvement compared to the previous work [16] from some of the authors. Physical simulations with human-in-the-loop demonstrate that 1) the approach enlarges sensibly the interaction working domain when compared to more standard inverse dynamics-based approaches, and 2) the proposed approach is very promising for a safe and effective future applications in human-aerial-robot physical interaction tasks on real-world systems, which is the next natural step after this work.

The paper is organized as follows. We start by describing the model of the aerial manipulator in Sec. II. The proposed control framework is then presented and detailed in section III. A number of simulation studies is provided in Sec. IV and some conclusive remarks are given in Sec. V.

II. Modelling

We consider an aerial robotic system composed of a *fully actuated aerial vehicle* endowed with a *robotic arm* possessing n_a Degrees of Freedom (DoFs). We shall refer to the full system as an *aerial manipulator* (AM), see Fig. 1 for an example.

The frames needed to describe the state of the AM are the *fixed world frame* $\mathcal{F}_W$ with unit axes $(\boldsymbol{x}_W, \boldsymbol{y}_W, \boldsymbol{z}_W)$ and origin O_W arbitrarily placed, the *aerial base frame* $\mathcal{F}_b$ with unit axes $(\boldsymbol{x}_b, \boldsymbol{y}_b, \boldsymbol{z}_b)$ and the origin O_b placed at the center of mass of the aerial vehicle, and the end effector frame $\mathcal{F}_E$ with unit axes $(\boldsymbol{x}_E, \boldsymbol{y}_E, \boldsymbol{z}_E)$ and the origin O_E rigidly attached to the *end effector* (EE) of the robotic arm.

The configuration of the AM is given by $\boldsymbol{q} = (\boldsymbol{p}_b, \boldsymbol{R}_b, \boldsymbol{q}_A) \in \mathcal{Q} \subseteq \mathbb{R}^3 \times SO(3) \times \mathbb{R}^{n_a}$. Where, $\boldsymbol{p}_b \in \mathbb{R}^3$ and $\boldsymbol{R}_b \in SO(3)$ represent the position and orientation of $\mathcal{F}_b$ with respect to $\mathcal{F}_W$, respectively, and $\boldsymbol{q}_A \in \mathbb{R}^{n_a}$ represents the arm joint angles. The AM pseudo-velocities are given by $\dot{\boldsymbol{q}} = [\boldsymbol{v}_b^\top \ \boldsymbol{\omega}_b^\top \ \boldsymbol{v}_A^\top]^\top \in \mathbb{R}^{6+n_a}$. Where, $\boldsymbol{v}_b \in \mathbb{R}^3 \in \mathbb{R}^3$ is the velocity of O_b expressed in $\mathcal{F}_W$, $\boldsymbol{\omega}_b \in \mathbb{R}^3$ is the angular velocity of $\mathcal{F}_b$ with respect to $\mathcal{F}_W$, expressed in $\mathcal{F}_b$, and $\boldsymbol{v}_A \in \mathbb{R}^{n_a}$ are the joints rates.

A. Kinematics

The position of O_E and the orientation of $\mathcal{F}_E$ with respect to $\mathcal{F}_W$ can be computed in terms of $\boldsymbol{q}$ using the Denavit-Hartenberg paramterization, and the differential kinematics can be used then to compute the EE instantaneous velocities $\dot{\boldsymbol{x}}_E = [\boldsymbol{v}_E^\top \ \boldsymbol{\omega}_E^\top]^\top \in \mathbb{R}^6$ as

$$\dot{\boldsymbol{x}}_E = \boldsymbol{J}(\boldsymbol{q})\dot{\boldsymbol{q}}, \tag{1}$$

where $\boldsymbol{J}(\boldsymbol{q})$ is the geometric Jacobian. Furthermore, the acceleration level differential kinematics, which is relevant to our proposed control scheme, is computed by taking the time derivative of (1)

$$\ddot{\boldsymbol{x}}_E = \boldsymbol{J}(\boldsymbol{q})\ddot{\boldsymbol{q}} + \dot{\boldsymbol{J}}(\boldsymbol{q}, \dot{\boldsymbol{q}})\dot{\boldsymbol{q}}. \tag{2}$$

B. Dynamics

By computing the kinetic and potential energy of the system and applying the Euler Lagrange formalism, the dynamic equations of the AM can be derived as

$$\boldsymbol{M}(\boldsymbol{q})\ddot{\boldsymbol{q}} + \boldsymbol{c}(\boldsymbol{q}, \dot{\boldsymbol{q}}) + \boldsymbol{g}(\boldsymbol{q}) = \left[\boldsymbol{w}_b^\top \boldsymbol{\tau}_A^\top\right]^\top + \boldsymbol{w}_{\text{ext}}, \tag{3}$$

where $\boldsymbol{M}(\boldsymbol{q}) \in \mathbb{R}^{(6+n_a)\times(6+n_a)}$ is the inertia matrix, $\boldsymbol{c}(\boldsymbol{q}, \dot{\boldsymbol{q}}) \in \mathbb{R}^{6+n_a}$ represents the Coriolis and centrifugal effects, and $\boldsymbol{g}(\boldsymbol{q}) \in \mathbb{R}^{6+n_a}$ is the gravity vector. The control wrench is represented by $\left[\boldsymbol{w}_b^\top \boldsymbol{\tau}_A^\top\right]^\top$ where $\boldsymbol{w}_b \in \mathbb{R}^6$ is the control wrench applied by/on the aerial vehicle, and $\boldsymbol{\tau}_A \in \mathbb{R}^3$ represents the input torques of the n_a-DoF arm. Lastly, $\boldsymbol{w}_{\text{ext}} \in \mathbb{R}^{6+n_a}$ represents the external forces or torques acting on the AM.

The actual system inputs of the aerial vehicle are the individual propeller thrust forces which can be related linearly to the squares of the propeller angular rates (see [17]) denoted with $\boldsymbol{w}_p \in \mathbb{R}^{n_p}$, where n_p is the number of propellers. The wrench mapping between $\boldsymbol{w}_b$ and $\boldsymbol{w}_p$ is given by a grasp-like matrix $\boldsymbol{G}_w \in \mathbb{R}^{6\times n_p}$, i.e.,

$$\boldsymbol{w}_b = \boldsymbol{G}_w \boldsymbol{w}_p. \tag{4}$$

Thanks to the full actuation assumption we have that $\boldsymbol{G}_w$ is full rank [17], which means that the applied wrench can be changed in all directions (locally). A global full actuation represents an ideal case, therefore we shall introduce both upper and lower bounds to the inputs to make the model much closer to the real situation, see later.

We assume that the only source of external forces and torques on the system is the collaborating human operator that interacts with the AM via the EE. Due to the duality between force and velocity, the relation between the human contact wrench $\boldsymbol{w}_h \in \mathbb{R}^6$ at the EE and $\boldsymbol{w}_{\text{ext}}$ is given by

$$\boldsymbol{w}_{\text{ext}} = \boldsymbol{J}(\boldsymbol{q})^\top \boldsymbol{w}_h. \tag{5}$$

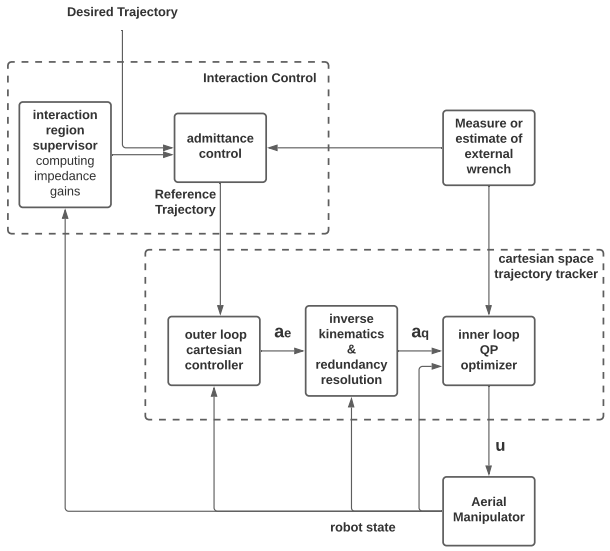

Fig. 2: Block diagram illustrating the proposed control framework.

Plugging (4) and (5) into (3) we obtain

$$\boldsymbol{M}(\boldsymbol{q})\ddot{\boldsymbol{q}} + \boldsymbol{c}(\boldsymbol{q},\dot{\boldsymbol{q}}) + \boldsymbol{g}(\boldsymbol{q}) = \boldsymbol{G}\boldsymbol{u} + \boldsymbol{J}(\boldsymbol{q})^\top \boldsymbol{w}_h, \tag{6}$$

Where $\boldsymbol{u} = \begin{bmatrix}\boldsymbol{w}_p^\top \boldsymbol{\tau}_A^\top\end{bmatrix}^\top$ are the actual system inputs and

$$\boldsymbol{G} = \begin{bmatrix}\boldsymbol{G}_w & \boldsymbol{0}_{6\times n_a} \\ \boldsymbol{0}_{n_a\times n_p} & \boldsymbol{I}_{n_a\times n_a}\end{bmatrix}. \tag{7}$$

Finally, for the sake of adherence with the real world conditions, we introduce the following input constraints:

$$\boldsymbol{u}_l \leq \boldsymbol{u} \leq \boldsymbol{u}_u, \tag{8}$$

where $\boldsymbol{u}_l$ and $\boldsymbol{u}_u$ are the lower and upper bounds of the input, respectively.

III. Methodology

The proposed control scheme is composed of several interconnected subsystems as depicted in Fig. 2. An *admittance controller* (also referred to as the *admittance filter*) is used to allow the AM to interact safely with a human. The parameters of the desired impedance dynamics used by the admittance controller are computed online by the *interaction region supervisor* based on the relative position of the robot and the human. The EE reference trajectory generated by the admittance filter is used by a *Cartesian space trajectory tracking controller*, which is divided in three stages. First, an *outer loop Cartesian controller*, including PD and feedforward terms, stabilizes the EE tracking error. Then the computed control effort at the EE is converted to the joint space via an *acceleration level inverse kinematics with a redundancy resolution* based on the projected gradient method. Lastly, at the inner most level of the controller, a constrained quadratic program is solved by the *inner loop Quadratic Program (QP) optimizer* to compute the system inputs taking into account the input limits. In the following we shall detail each component of the proposed scheme.

A. Cartesian Space Trajectory Tracking

Consider a full pose trajectory tracking task (task dimension $m = 6$) for the EE of the AM given by $\boldsymbol{x}_E^r = (\boldsymbol{p}_E^r, \boldsymbol{R}_E^r)$, where $\boldsymbol{p}_E^r \in \mathbb{R}^3$ is the reference position of the EE and $\boldsymbol{R}_E^r \in SO(3)$ represents the reference orientation of the EE.

The inner loop QP optimizer solves the convex QP

$$\underset{\boldsymbol{u}}{\text{minimize}} \quad \frac{1}{2}\boldsymbol{u}^\top \boldsymbol{P}\boldsymbol{u} + \boldsymbol{f}^\top \boldsymbol{u} \tag{9a}$$

$$\text{subject to:} \quad \boldsymbol{u}_l \leq \boldsymbol{u} \leq \boldsymbol{u}_u \tag{9b}$$

where,

$$\boldsymbol{P} = (\boldsymbol{M}^{-1}(\boldsymbol{q})\boldsymbol{G})^\top (\boldsymbol{M}^{-1}(\boldsymbol{q})\boldsymbol{G})$$

$$\boldsymbol{f}^\top = (\boldsymbol{h} - \boldsymbol{a}_q)^\top \boldsymbol{M}^{-1}(\boldsymbol{q})$$

$$\boldsymbol{h} = \boldsymbol{M}^{-1}(\boldsymbol{q})(-\boldsymbol{c}(\boldsymbol{q},\dot{\boldsymbol{q}}) - \boldsymbol{g}(\boldsymbol{q}) + \boldsymbol{w}_{\text{ext}}).$$

Such optimizer, which is the innermost loop of the control scheme, is tasked to compute the system inputs that minimize the quadratic objective $(\ddot{\boldsymbol{q}} - \boldsymbol{a}_q)^\top (\ddot{\boldsymbol{q}} - \boldsymbol{a}_q)$, where $\boldsymbol{a}_q$ is a virtual input provided by the adjacent outer loop, i.e., the inverse kinematics and redundancy resolution (see Fig. 2).

In the ideal case, (i.e., the optimal input would achieve $\ddot{\boldsymbol{q}} = \boldsymbol{a}_q$) the optimal solution is input-output decoupling and linearizing. However, in that case, we do not achieve exact feedback linearization, since for a fully actuated AM with $n_a > 0$, the robot is redundant with respect to a full pose tracking task, and there exist an $(6 + n_a) - m$-dimensional internal dynamics, This aspect is taken care by the redundancy resolution subsystem, described below.

The virtual input $\boldsymbol{a}_q$ is computed by first computing the EE tracking error vector $\boldsymbol{a}_e = \begin{bmatrix}\boldsymbol{a}_{e_1}^\top \boldsymbol{a}_{e_2}^\top\end{bmatrix}^\top$ as

$$\boldsymbol{a}_{e_1} = \ddot{\boldsymbol{p}}_e^r + \boldsymbol{K}_{P_1}(\dot{\boldsymbol{p}}_e^r - \dot{\boldsymbol{p}}_e) + \boldsymbol{K}_{P_2}(\boldsymbol{p}_e^r - \boldsymbol{p}_e) \tag{11}$$

$$\boldsymbol{a}_{e_2} = \dot{\boldsymbol{\omega}}_e^r + \boldsymbol{K}_{\omega_1}(\boldsymbol{\omega}_e^r - \boldsymbol{\omega}_e) + \boldsymbol{K}_{\omega_2}\boldsymbol{e}_R \tag{12}$$

with the orientation error defined as

$$\boldsymbol{e}_R = \frac{1}{2}[\boldsymbol{R}_e^T \boldsymbol{R}_e^r - \boldsymbol{R}_e^{r^T} \boldsymbol{R}_e]_\vee. \tag{13}$$

This computation is referred to as outer loop Cartesian controller in the block diagram (see Fig. 2).

The redundancy resolution subsystem then computes $\boldsymbol{a}_q$ as follows

$$\boldsymbol{a}_q = \boldsymbol{J}_W^\dagger(\boldsymbol{q})(\boldsymbol{a}_e - \dot{\boldsymbol{J}}(\boldsymbol{q},\dot{\boldsymbol{q}})\dot{\boldsymbol{q}}) + \big(\boldsymbol{I}_{6+n_a} - \boldsymbol{J}_W^\dagger(\boldsymbol{q})\boldsymbol{J}(\boldsymbol{q})\big)\boldsymbol{a}_z, \tag{14}$$

where, $\boldsymbol{J}_W^\dagger(\boldsymbol{q})$ represents the weighted pseudoinverse of $\boldsymbol{J}(\boldsymbol{q})$ computed as $\boldsymbol{J}_W^\dagger(\boldsymbol{q}) = \boldsymbol{W}^{-1}\boldsymbol{J}(\boldsymbol{q})^\top(\boldsymbol{J}(\boldsymbol{q})\boldsymbol{W}^{-1}\boldsymbol{J}(\boldsymbol{q})^\top)^{-1}$, and $\boldsymbol{W}$ is a weight matrix that affects the distribution of motion over the joint space variables taking into account the AM capabilities. As discussed by the authors of [18], the weights can be chosen such that navigation tasks are performed mainly by the aerial vehicle while manipulation tasks are executed mainly by the n_a-dof arm. The task Jacobian $\boldsymbol{J}(\boldsymbol{q})$ possesses a $(6 + n_a) - m$ dimensional null space, which

can be exploited by projecting an additional virtual input $\boldsymbol{a}_z$ in the null space by means of the null space projector $\left(\boldsymbol{I}_{6+n_a} - \boldsymbol{J}_W^{\dagger}(\boldsymbol{q})\boldsymbol{J}(\boldsymbol{q})\right)$. The vector $\boldsymbol{a}_z$ represents the preferred joint-space accelerations to be executed in the null space of $\boldsymbol{J}(\boldsymbol{q})$.

To design $\boldsymbol{a}_z$ we use the projected gradient approach [19], in which desired behaviors are represented as optimization criteria of some objective functions. The weighted sum of the gradients of these functions is then projected in the null space using (14). A term that stabilizes the internal dynamics is also added to $\boldsymbol{a}_z$ by default.

In general, to keep a variable x as close as possible to the midpoint of its operating range $x \in [x_l, x_u]$ the following objective function can be used

$$H_{\mathrm{r}}(x) = \frac{1}{2}\left(\frac{x - \bar{x}}{x_u - x_l}\right)^2, \tag{15}$$

where $\overline{x} = \frac{x_u + x_l}{2}$.

As discussed in [20], for a uni-directional thrust fully actuated aerial vehicle – i.e., the typical aerial vehicle possess propellers that can produce force in only one direction – it is important to keep the platform tilt angles (i.e., the roll and pitch) within an operating range to avoid generating unfeasible thrust commands. Consequently, we use two objective functions similar to (15) – namely $H_{\mathrm{r}}(\phi)$ and $H_{\mathrm{r}}(\theta)$ where ϕ and θ are the roll and pitch angles respectively extracted from $\boldsymbol{R}_b$ – to favor configurations with tilt angles that are close to zero. Similarly, we use $H_{\mathrm{r}}(\boldsymbol{q}_{A_i})$ to favor configurations in which the i^{th} joint angle of the arm within is in the middle of its range, for all $i = 1, \ldots, n_a$. Finally, a_z is computed as follows

$$\boldsymbol{a}_z = \frac{1}{2 + n_a}\nabla H - \boldsymbol{K}_n \dot{\boldsymbol{q}} \tag{16}$$

$$\nabla H = \left(-k_1 \nabla_{\phi} H_{\mathrm{r}}(\phi) - k_2 \nabla_{\theta} H_{\mathrm{r}}(\theta) - \sum_{i=1}^{n_a} k_i \nabla_{\boldsymbol{q}_{A_i}} H_{\mathrm{r}}(\boldsymbol{q}_{A_i})\right)$$

where, $\boldsymbol{K}_n \in \mathbb{R}^{(6+n_a)\times(6+n_a)}$ is a positive definite diagonal matrix, and k_1, k_2, and the k_i's are positive scalar gains that define a priority between the gradients.

B. Interaction Control

1) Admittance Control: Impedance and admittance control schemes, initially described in the seminal work [21], allow to shape the interaction forces when interacting with an unknown environment. By modeling the interaction as a multidimensional mass-spring-damper system, and then choosing the appropriate values for the apparent inertia, damping, and stiffness, the interaction between a human operator and a robot can be made safe and intuitive/ergonomic.

We assume that an external planner (whose design is out of the scope of this work this scheme) provides a desired EE trajectory $\boldsymbol{x}_e^d = (\boldsymbol{p}_e^d, \boldsymbol{R}_e^d)$, where $\boldsymbol{p}_e^d \in \mathbb{R}^3$ is the desired position of the EE and $\boldsymbol{R}_e^d \in SO(3)$ represents its desired orientation. The admittance control changes the desired EE trajectory by computing the desired (apparent) impedance dynamics given by

$$\mathbf{M}_E \Delta\dot{\boldsymbol{v}}_E + \mathbf{D}_E \Delta\boldsymbol{v}_E + \mathbf{K}_E \mathbf{e}_E = \boldsymbol{w}_h \tag{17}$$

where $\Delta\boldsymbol{v}_E = \dot{\boldsymbol{p}}_e^d - \dot{\boldsymbol{p}}_e^r$ is the velocity error and the pose error $\mathbf{e}_E$ is given by

$$\mathbf{e}_E = \begin{bmatrix} \mathbf{p}_e^d - \mathbf{p}_e^r \\ \frac{1}{2}\left(\mathbf{R}_e^d \mathbf{R}_e^{r^{\mathrm{T}}} - \mathbf{R}_e^r \mathbf{R}_e^{d^{\mathrm{T}}}\right)^{\vee} \end{bmatrix} \tag{18}$$

The result is the reference trajectory that is tracked by the motion controller described in Sec. III-A.

2) Interaction Region Supervisor: We assume that the environment where an aerial manipulator would collaborate and interact with a human operator is limited in size, particularly since human operators working at great heights like power transmission lines are usually inside crane boxes or attached with ropes. We choose arbitrary shapes that are defined apriori around the human operator, which we call *interaction regions*.

The interaction region supervisor (see Fig. 2) is in charge of modifying the apparent stiffness $\mathbf{K}_E$ of the impedance dynamics (17) based on the position of the EE within the interaction region. In particular, inside the interaction region the apparent stiffness is *made very light* so that the robot can be guided freely by the human operator. If the robot is driven out of the interaction region, the robot apparent stiffness increases quadratically to bring the robot back to the edge of the interaction region, where it is *within reach* of the human operator.

IV. Results of Numerical Investigations

In this section, we investigate the properties of the proposed control scheme and validate its performance in a number of different simulations. Our objective with the presented simulation studies is to assess the behavior of the AM under the influence of interaction forces, with possible input saturations, in an pHRI scenario. The AM platform used in the simulation is modeled after a real platform designed at the Robotics and Mechatronics lab at the University of Twente, see Fig. 1. The fully actuated aerial vehicle is a fixedly tilted-propeller hexarotor, hence $n_p = 6$. A lightweight 3-DoF arm (i.e., $n_a = 3$) is mounted below the aerial vehicle. The arm alone weights 1 Kg and its mass-to-payload ratio is $1:1$. The robot has in total 9 DoFs and therefore it is redundant with respect to the end effect task, which is 6 dimensional.

A. QP versus Post-saturated Feedback Linearization

As mentioned in Sec. III, in the ideal case – i.e., without input saturation – the optimal input is the feedback linearizing one, and a standard feedback linearization scheme based on inverse dynamics would suffice to solve the Cartesian space EE tracking problem. However, during physical interaction between the aerial manipulator and a human – and in general this holds for any uncontrolled environment – the force exchanges with the human might lead to input saturation in the real robotic system. Even the more so when considering the limited actuation capabilities of aerial manipulators. In such cases each entry of the input computed by the feedback linearization that exceeds the corresponding entry of the input limits $\boldsymbol{u}_l$ or $\boldsymbol{u}_u$ would be saturated by the system itself, regardless of what the feedback linearization

PSFL vs QP: maximum tracking squared error norm		
External force intensity	PSFL max squared pose error norm	QP max squared pose error norm
5 N	0.0	0.0
6 N	127.2	0.9
7 N	176.1	36.4
8 N	190.5	132.7
9 N	850.6	339.0
$\geq$ 10 N	unstable	stable until 25 N

TABLE I: Comparison between the maximum values of squared pose error norm of the EE tracking during when the AM is controlled by a Post-saturated Feedback Linearization (a.k.a. Inverse Dynamics) compared to the proposed QP-based approach.

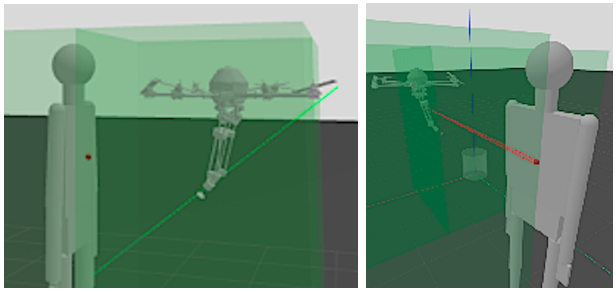

Fig. 3: Human-in the Loop Simulations of Physical Interaction. In transparent green the interaction region, the green line is the desired trajectory, and the red line represents the direction and magnitude of the force applied by a real human operating the joystick during the simulation.

controller asks to the system. Therefore, we refer to the feedback linearization approach with the more accurate term of *post-saturated feedback linearization* (PSFL).

The natural question is therefore whether our approach performs better than a simpler PSFL approach, i.e., if the added complexity pays off. Such question is of fundamental importance because the more the Cartesian tracker is able to minimize the tracking error the more the overall compliant control scheme is able to mimic the desired impedance therefore resulting in a behavior which is more predictable, more ergonomic, and safer for the human operator.

In order to answer such question, we conducted a numerical simulation campaign that compares the proposed scheme and a PSFL one. In such campaign we task the AM to remain still in a homing configuration while we incrementally increase the interaction force. To achieve so we set $\boldsymbol{w}_h = \begin{bmatrix} w_{hx}(t) & \mathbf{0}_{1\times 5}^\top \end{bmatrix}$ and choose $w_{hx}(t)$ as a train of five force pulses where each pulses lasts 1 s, and whose amplitude increases from 5 N with steps of 1 N, until the system can remain stable under the action of such interaction force, which acts as a disturbance. We assume that a measure or an estimate of such force is available to the AM. This measure is used within both control schemes inside (3) and (5). We apply the aforementioned interaction wrench to the same AM controlled once with the proposed approach and then with the PSFL approach and we record the corresponding maximum value of squared pose error norm of the EE tracking, i.e., $\mathbf{e}_E^\top \mathbf{e}_E$. We encourage the reader to watch the multimedia attachment to see how such simulation is performed.

The results of the simulation campaign are gathered in Table I and show a clear superiority of the proposed approach when compared to the PSFL one. With a disturbance force of magnitude less or equal to $5N$, both schemes are able to counteract the the disturbance without saturating the AM actuators and resulting in zero tracking errors. As the disturbance force increases, the QP-based scheme obtains a sensibly lower maximum tracking error compared to the PSFL and a nicer degradation of the tracking performances.

The second result is that when applying an external force of 9 N, or larger, the PSFL scheme fails in controlling the platform, while the QP based scheme is able to maintain a stable flight subject to an external force of up to 25 N, i.e., the proposed approaches enlarges the range of feasible interaction forces by almost thee times. It reasonable to infer that interaction forces that are larger than 25 N cannot be handled by the simulated platform because of the limited nature of the inputs which makes the stabilization task practically impossible with that amount of disturbance.

B. Human-in the Loop Simulations of Physical Interaction

To show the effectiveness of the full control scheme in a human interaction-like scenario we used a Gazebo environment. The control scheme is implemented on Matlab/Simulink, with the interfacing between the controller and the robot being managed by combination of Gazebo-yarp and Gazebo-genom3 plugins. The physics of the aerial manipulator is instead computed by Gazebo, using the ODE physics engine, thus avoiding to validate the controller with the same equations that we used to implement the controller itself, which is a good practice in simulation, see Fig. 3. Additionally, we developed a Gazebo plugin which converts human commands provided online by a real human from a joystick to forces applied at the EE of the robot.

1) Simulation scenario: Navigation, Interaction and Collision: The first simulation depicts a scenario composed of three phases, referred to as *Navigation*, *Interaction* and *Collision*, respectively. In the Navigation phase AM follows a desired EE trajectory close to the human and then stops in front of the human co-worker, just inside the interaction region. Then the Interaction phase starts, in which the human co-worker guides the AM freely inside the interaction space, where the interaction dynamics supervisor imposes the appropriate stiffness for such region, which is chosen to be very small. Lastly, during the Collision phase, a relatively large force – simulating an accidental contact between the human operator and the AM – drives some of the robot inputs to saturation.

The EE reference tracking in the navigation phase can be seen in the first portion of the plots of Figs. 4 and 5. The Cartesian space trajectory tracking controller successfully achieves its task.

The interaction phase is then started when the human operator, intentionally, applies forces to the robot. The interaction forces by the human operator are displayed in Fig. 6. The effect of the interaction control subsystem can be seen by inspecting Figs. 7 and 4, during the Interaction phase. The desired trajectories are modified by the admittance filter (see Fig. 7) to produce reference trajectories that attain the desired

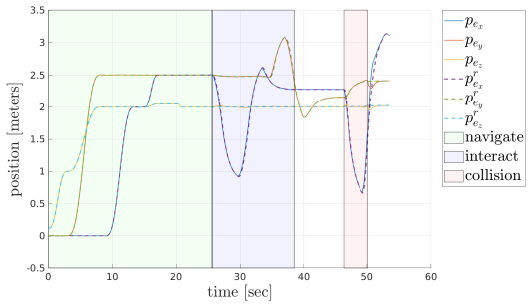

Fig. 4: Scenario 1: The evolution of the EE position throughout the three phases of the Navigation, Interaction and Collision simulation.

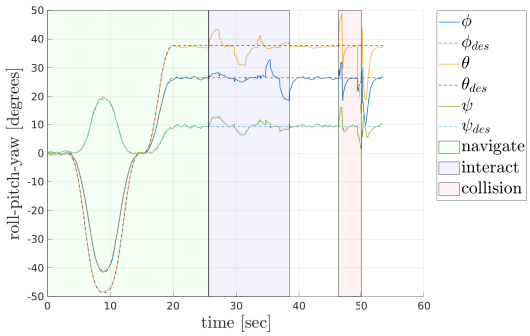

Fig. 5: Scenario 1: The evolution of the EE orientation throughout the three phases of the Navigation, Interaction and Collision simulation.

apparent compliant behavior. These trajectories are tracked as closely as possible by the motion tracker, which can be observed in the corresponding section of Fig. 4.

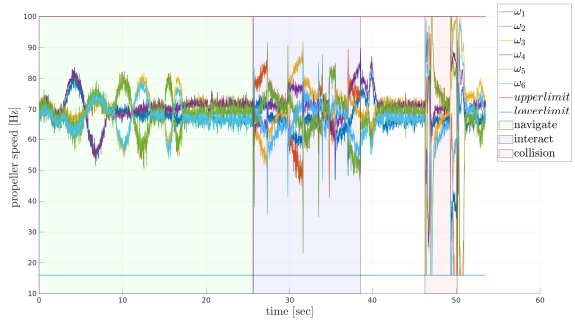

Fig. 8: Scenario 1: The propeller speeds which are the actual inputs to the aerial vehicle. Note the input saturation in the collision phase.

Lastly, the collision phase starts when the human operator applies abruptly a force of approximately 11 N to the AM, two times consecutively, simulating accidental contacts. This leads to saturation some of the propeller inputs as shown in Fig. 8. However, as it can be appreciated the AM is not destabilized by this event and is able to recover.

V. Conclusions

In conclusion, in this paper we proposed a control framework to enable physical human robot interaction for aerial manipulators, where it is very important to consider actuation

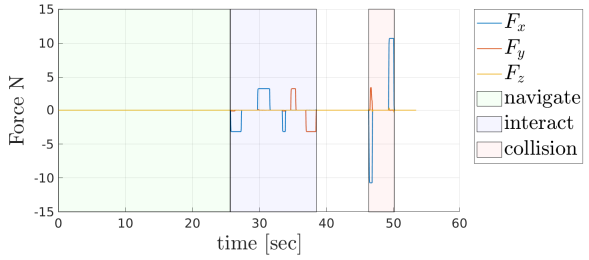

Fig. 6: Scenario 1: The inputs provided online by the human in-the-loop via the joystick and applied at the EE of the robot.

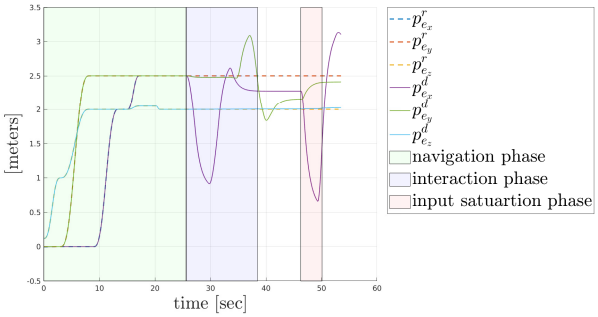

Fig. 7: Scenario 1: The desired trajectory which is the input to the admittance filter is plotted vs the output of the filter which is the reference trajectory.

constrains. The framework is composed of and optimization based Cartesian space trajectory tracking controller, it resolves the redundancy by incrementally optimizing some objective functions and taking into account operating ranges. The scheme is then combined with an admittance filter for safe physical human robot interaction and an interaction region supervisor for taking into account the needs of different interaction modalities depending on mutual position with respect to the human co-worker. The system was validated in simulation, and the results show the viability of the approach to aerial manipulator physically interacting with humans.

Future work will be mainly focused on the experimental test of the proposed framework on the real prototype depicted in Fig. 1, which will include the use of on board sensors for tasks such as force measurement, human intention understanding, and interaction region detection, among others. In order to realize and test the proposed control framework on the real AM prototype, we expect some challenges that are particularly interesting to the practitioners in the domain of physical aerial interaction. One of the most notable challenges is the operational mode of the actuators of the attached robotic arm. Due to payload restrictions on aerial platforms, torque controlled robotic arms are not always possible, alternatively, position and velocity controlled motors are used. There has been a few examples in the literature that have tackled this issue in different ways, see [16] and [22]. However, in these works, the AM control was done in joint space with no exploitation of redundancy. It will be interesting, to evaluate the Cartesian space controller performance with the methods proposed in the previous works.

REFERENCES

[1] A. Ollero, M. Tognon, A. Suarez, D. J. Lee, and A. Franchi, "Past, present, and future of aerial robotic manipulators," *IEEE Trans. on Robotics*, 2021.

[2] A. Ollero, G. Heredia, A. Franchi, G. Antonelli, K. Kondak, A. Sanfeliu, A. Viguria, J. R. Martinez-de Dios, F. Pierri, J. Cortés, A. Santamaria-Navarro, M. A. Trujillo, R. Balachandran, J. Andrade-Cetto, and A. Rodriguez, "The AEROARMS project: Aerial robots with advanced manipulation capabilities for inspection and maintenance," *IEEE Robotics & Automation Magazine, Special Issue on Floating-base (Aerial and Underwater) Manipulation*, vol. 25, no. 4, pp. 12–23, 2018.

[3] M. Tognon, H. A. Tello Chávez, E. Gasparin, Q. Sablé, D. Bicego, A. Mallet, M. Lany, G. Santi, B. Revaz, J. Cortés, and A. Franchi, "A truly redundant aerial manipulator system with application to push-and-slide inspection in industrial plants," *IEEE Robotics and Automation Letters*, vol. 4, no. 2, pp. 1846–1851, 2019.

[4] E. Cataldi, G. Muscio, M. A. Trujillo, Y. Rodriguez, F. Pierri, G. Antonelli, F. Caccavale, A. Viguria, S. Chiaverini, and A. Ollero, "Impedance control of an aerial-manipulator: Preliminary results," in *2016 IEEE/RSJ Int. Conf. on Intelligent Robots and Systems*, 2016, pp. 3848–3853.

[5] J. Welde, J. Paulos, and V. Kumar, "Dynamically feasible task space planning for underactuated aerial manipulators," *IEEE Robotics and Automation Letters*, vol. 6, no. 2, pp. 3232–3239, 2021.

[6] S. Haddadin, A. De Luca, and A. Albu-Schäffer, "Robot collisions: A survey on detection, isolation, and identification," *IEEE Transactions on Robotics*, vol. 33, no. 6, pp. 1292–1312, 2017.

[7] A. De Luca and F. Flacco, "Integrated control for phri: Collision avoidance, detection, reaction and collaboration," in *2012 4th IEEE RAS EMBS International Conference on Biomedical Robotics and Biomechatronics (BioRob)*, 2012, pp. 288–295.

[8] A. Ajoudani, A. M. Zanchettin, S. Ivaldi, A. Albu-Schäffer, K. Kosuge, and O. Khatib, "Progress and prospects of the human–robot collaboration," *Autonomous Robots*, vol. 42, no. 5, pp. 957–975, 2018.

[9] F. Augugliaro and R. D'Andrea, "Admittance control for physical human-quadrocopter interaction," in *2013 European Control Conference*, 2013, pp. 1805–1810.

[10] T. Tomić, C. Ott, and S. Haddadin, "External wrench estimation, collision detection, and reflex reaction for flying robots," *IEEE Transactions on Robotics*, vol. 33, no. 6, pp. 1467–1482, 2017.

[11] M. Tognon, R. Alami, and B. Siciliano, "Physical human-robot interaction with a tethered aerial vehicle: Application to a force-based human guiding problem," *IEEE Transactions on Robotics*, vol. 37, no. 3, pp. 723–734, 2021.

[12] A. Suarez, P. Sanchez-Cuevas, M. Fernandez, M. Perez, G. Heredia, and A. Ollero, "Lightweight and compliant long reach aerial manipulator for inspection operations," in *2018 IEEE/RSJ Int. Conf. on Intelligent Robots and Systems*, 2018, pp. 6746–6752.

[13] L. Yuan, C. Reardon, G. Warnell, and G. Loianno, "Human gaze-driven spatial tasking of an autonomous mav," *IEEE Robotics and Automation Letters*, vol. 4, no. 2, pp. 1343–1350, 2019.

[14] L. Peric, M. Brunner, K. Bodie, M. Tognon, and R. Siegwart, "Direct force and pose nmpc with multiple interaction modes for aerial push-and-slide operations," in *2021 IEEE Int. Conf. on Robotics and Automation*, 2021, pp. 131–137.

[15] D. Bicego, J. Mazzetto, M. Farina, R. Carli, and A. Franchi, "Nonlinear model predictive control with enhanced actuator model for multi-rotor aerial vehicles with generic designs," *Journal of Intelligent & Robotics Systems*, vol. 100, pp. 1213–1247, 2020.

[16] G. Nava, Q. Sablé, M. Tognon, D. Pucci, and A. Franchi, "Direct force feedback control and online multi-task optimization for aerial manipulators," *IEEE Robotics and Automation Letters*, vol. 5, no. 2, pp. 331–338, 2020.

[17] M. Hamandi, F. Usai, Q. Sable, N. Staub, M. Tognon, and A. Franchi, "Design of multirotor aerial vehicles: a taxonomy based on input allocation," *The International Journal of Robotics Research*, vol. 40, no. 8-9, pp. 1015–1044, 2021.

[18] A. Santamaria-Navarro, V. Lippiello, and J. Andrade-Cetto, "Task priority control for aerial manipulation," in *2014 IEEE International Symposium on Safety, Security, and Rescue Robotics*, 2014, pp. 1–6.

[19] A. Luca, G. Oriolo, and B. Siciliano, "Robot redundancy resolution at the acceleration level," *Laboratory Robotics and Automation*, vol. 4, pp. 97–106, 01 1992.

[20] M. Ryll, D. Bicego, and A. Franchi, "A truly redundant aerial manipulator exploiting a multi-directional thrust base," in *2018 IFAC Symp. on Robot Control*, Budapest, Hungary, Aug. 2018, pp. 138–143.

[21] N. Hogan, "Impedance control: An approach to manipulation," in *1984 American Control Conference*.

[22] K. Bodie, M. Tognon, and R. Siegwart, "Dynamic end effector tracking with an omnidirectional parallel aerial manipulator," *IEEE Robotics and Automation Letters*, vol. 6, no. 4, pp. 8165–8172, 2021.